Applied Catalysis B: Environmental 192 (2016) 171–181

Contents lists available at ScienceDirect

Applied Catalysis B: Environmental

journal homepage: www.elsevier.com/locate/apcatb

Characterization and catalytic performance of hydrotalcite-derived Ni-Cu alloy nanoparticles catalysts for steam reforming of 1-methylnaphthalene

Dalin Li[a,*], Miaomiao Lu[a], Kosuke Aragaki[b], Mitsuru Koike[b], Yoshinao Nakagawa[b], Keiichi Tomishige[b,*]

[a] National Engineering Research Center of Chemical Fertilizer Catalyst (NERC-CFC), School of Chemical Engineering, Fuzhou University, Gongye Road No.523, Fuzhou 350002, Fujian, PR China
[b] Department of Applied Chemistry, School of Engineering, Tohoku University, 6-6-07, Aoba, Aramaki, Aoba-ku, Sendai 980-8579, Japan

ARTICLE INFO

Article history:
Received 26 November 2015
Received in revised form 22 March 2016
Accepted 24 March 2016
Available online 26 March 2016

Keywords:
Gasification
Tar
Steam reforming
Hydrotalcite-like compounds
Nickel-copper alloy

ABSTRACT

Supported Ni-Cu alloy nanoparticles prepared from Ni-Cu-Mg-Al hydrotalcite-like compounds (HTlcs) with Cu/Ni = 0.25 have been shown to be an active catalyst for the steam reforming of tar derived from the biomass pyrolysis. In the present work, Ni-Cu alloy catalysts with wider compositions of Cu/Ni were characterized and their performances were evaluated in the steam reforming of 1-methylnaphthalene (1-MN), which has lower reactivity than the biomass tar, in order to make the effect of Cu/Ni much clearer. The characterizations with XRD, STEM-EDX, H_2 chemisorption, and FIIR of CO adsorption suggest that the obtained Ni-Cu alloy nanoparticles had uniform composition in the range of Cu/Ni = 0.1–1; the particle size was decreased with the increase of Cu/Ni ratio (ca. 5–7 nm), and Cu tended to be enriched on the particle surface. The HTlcs-derived Ni-Cu alloy catalysts showed a volcano-type dependence of activity on the alloy composition; the highest reforming activity and lower yields of byproducts including benzene, naphthalene, and coke were obtained at Cu/Ni = 0.25. The kinetic study indicates that 1-MN was strongly adsorbed on both the Ni and Ni-Cu catalysts; in contrast, the adsorption of steam was promoted by the alloying of Ni with Cu even in the presence of strongly adsorbed 1-MN. The property of stronger adsorption of steam can be connected to higher reforming activity and lower coke deposition through the dissociative adsorption of steam to supply more adsorbed oxygen species, which enhance the gasification of carbonaceous species.

1. Introduction

Gasification is one of the most important technologies for clean and high efficient utilization of solid carbon resources such as coal, petroleum coke, and biomass [1,2]. Gasification is a thermal chemical conversion process producing a fuel gas rich in hydrogen and carbon monoxide. The product gas or synthesis gas ($CO + H_2$) has great application potentials for electricity generation, hydrogen production, and synthesis of chemicals and liquid fuels. However, the raw product gas from the gasifier contains many contaminants. Particularly, the presence of tar by-product is highly undesired. Tar is a complex mixture of organic compounds, including monocyclic and polycyclic aromatic hydrocarbons as well as other oxygen-containing hydrocarbons, e.g., benzene, toluene, naphthalene, phenol, etc. [2]. Tar can condense in the gasifier pipe outlets and in particulate filters leading to blockages and filter clogging. It causes further downstream problems and clogs fuel lines and injectors in internal combustion engines. Moreover, tar would cause serious coke deposition on the downstream catalyst if the synthesis gas is used for the production of liquid fuels and chemicals. Therefore, considerable efforts have been devoted to the development of effective methods for tar removal. Among the different methods, the catalytic steam reforming of tar seems to be very promising, since it can convert tar into useful gaseous products, not only improving the synthesis gas quality and overall energy efficiency, but also avoiding the need for the collection and disposal of tar as well as tar pollution [3,4].

Supported metal catalysts including Ni, Co, Fe, and noble metals such as Rh have been widely studied for the steam reforming

* Corresponding authors.
E-mail addresses: dalinli@fzu.edu.cn (D. Li), tomi@erec.che.tohoku.ac.jp (K. Tomishige).

http://dx.doi.org/10.1016/j.apcatb.2016.03.052
0926-3373/

of tar and its model compounds, e.g., benzene, toluene, phenol, naphthalene, and 1-methylnaphthelene (1-MN) [5–12]. Owing to its relatively low cost and high activity, the Ni catalyst has attracted much attention. However, the main problem of Ni catalyst is the deactivation caused by the coke deposition and agglomeration of Ni metal particles. Alloying Ni with other transition metals (Pt, Rh, Pd, Ru, Fe, Co) [6,13–18] has been applied to improve the catalyst activity, stability, and coke resistance. Particularly, alloying Ni with non-precious metals such as Fe [6,14–17] and Co [18] appears attractive, which exhibits better performance than the corresponding monometallic catalysts. Typically, the alloy catalysts were prepared by the impregnation method. However, this method usually gave large metal particles and weak interaction between metal particles and support. Moreover, it may cause large inhomogeneity in the composition of the alloy particles, leading to the formation of alloy particles with different structures such as *fcc* alloy, *bcc* alloy, and/or intermetallic compounds [14,18,19]. Since the catalytic performance of alloy particles are greatly dependent on their structure, composition, and particle size, the preparation of uniform alloy nanoparticles catalyst is critical for the catalytic performance.

Utilization of hydrotalcite-like compounds (HTlcs) as precursor offers a feasible route for the controlled preparation of alloy catalysts [20–22]. HTlcs, also known as layer double hydroxides (LDHs), are a class of anionic clays that consist of positively charged two-dimensional brucite-like sheets in which a fraction of the divalent cations are isomorphously substituted by trivalent cations, together with charge-compensating anions and water in the interlayer [23]. Owing to their versatility in chemical composition and uniform distribution of cations in the brucite layers, HTlcs have been widely used as precursors of metal catalysts [24–26]. By incorporating Ni^{2+} and Fe^{3+} into the Mg-Al HTlcs, followed by calcination and reduction treatments, we have successfully prepared a well dispersed Ni-Fe alloy catalyst with single phase and rather uniform composition [20,21]. The HTlcs-derived uniform Ni-Fe alloy catalyst showed superior performance for the steam reforming of biomass tar than the Ni-Fe/α-Al_2O_3 catalyst prepared by the conventional impregnation method in terms of activity, stability, coke resistance and regenerability, demonstrating the advantage of using HTlcs as precursor for tuning the alloy structure and catalytic performance.

Recently, we explored this strategy to prepare a uniform Ni-Cu alloy catalyst from Ni-Cu-Mg-Al HTlcs [27], and the uniform Ni-Cu alloy nanoparticles obtained at Cu/Ni = 0.25 showed high performance in the steam reforming of tar from the biomass pyrolysis. The performance was comparable or even higher than that of HTlcs-derived Ni-Fe alloy catalyst [21]. Therefore, it is important to investigate the structural property and catalytic performance of the HTlcs-derived Ni-Cu alloy catalysts in details. However, regarding the comparison of various Ni-Cu catalysts with different compositions in terms of the catalytic performance, the tar from the biomass pyrolysis is not suitable because of its high reactivity, which makes the performance difference smaller [27]. In order to make the difference clearer, the model substrate with lower reactivity was used in the present work. In the previous reports [10–12], 1-methylnaphthalene (1-MN) has been used as model compound of tar, which is a representative poly-aromatic component of tar and is among the most difficult to convert. The effects of alloy compositions and reaction parameters including Cu/Ni ratio, contact time, reactant partial pressure, and time on stream were investigated and the catalysts before and after reaction were characterized by various techniques. In particular, the utilization of 1-MN enabled the kinetic study, although the kinetic study is difficult in the case of biomass tar due to the mixture of various compounds [27]. The kinetic study can give the information on the adsorption strength of the substrates and their coverage. Based on these results, the relationship between the alloy structure and catalytic performance was discussed; in particular, the kinetic study made the role of Cu clearer.

2. Experimental

2.1. Catalyst preparation

All the chemicals used in this work were of analytical grade (Wako Pure Chemical Industries). Ni-Cu-Mg-Al HTlcs were synthesized by co-precipitation method as reported previously [27]. In brief, a 100 mL aqueous solution of mixed nitrates ($Ni(NO_3)_2{\cdot}6H_2O$, $Cu(NO_3)_2{\cdot}3H_2O$, $Mg(NO_3)_2{\cdot}6H_2O$, and $Al(NO_3)_3{\cdot}9H_2O$) was dropwise added to 100 mL aqueous solution of Na_2CO_3 under vigorously stirring. The pH of the solution was adjusted with an aqueous solution of NaOH (2 M) and kept constant at 10 ± 0.5. The solid product thus obtained was recovered by filtration followed by washing and drying at 383 K. Ni-Cu/Mg/Al samples were obtained by calcination at 1073 K for 5 h in air to decompose the HTlcs precursor. The molar ratio of (Ni + Cu + Mg)/Al was kept at 3, and the Ni content was fixed at 12.0 wt% as a weight percentage in the calcined sample, whereas the Cu content varied from 1.3 to 13.0 wt% to obtain a molar ratio of Cu/Ni between 0.1 and 1.0. For comparison, two monometallic catalysts, i.e., Ni/Mg/Al and Cu/Mg/Al with 12.0 wt% metal content were also prepared by a similar procedure described above. The detailed chemical compositions of the samples are listed in Table S1 (Supplementary material).

2.2. Catalytic reaction

Steam reforming of 1-MN was conducted in a fixed-bed flow reactor. A quartz tube (inner diameter 4 mm) was used as the reactor. The reaction temperature was monitored with a thermocouple located at the catalyst bed outlet. The catalyst was pre-reduced with a H_2/N_2 ($30/30\,mL\,min^{-1}$) gas flow at 1073 K for 0.5 h. After the reduction treatment, the reactor was purged with N_2, and the temperature was increased to 1123 K. Subsequently, both steam and 1-MN were introduced to the catalyst bed, which were supplied by two syringe pumps, respectively, followed by vaporization in a heating chamber at 673 K with N_2 as the carrier gas. The effluent gas passed through an iced water condenser loaded with mesitylene to trap 1-MN, naphthalene, toluene, benzene, and other liquid products. The sample of gaseous products was taken by a syringe and analyzed by gas chromatograph (GC). The H_2 concentration was determined by TCD-GC (Molecular sieve 13×), and the concentrations of CO, CH_4, and CO_2 were measured by FID-GC (Gaskuropack 54) equipped with a methanator. The total flow rate of the gaseous products was measured by a bubble flow meter. To determine the concentrations of 1-MN, naphthalene, toluene, and benzene, the trapped solution was analyzed by FID-GC (InertCap 5MS/Sil) using *n*-heptane as an internal standard. After reaction, supplies of 1-MN and steam were stopped, and oxygen was introduced to the catalyst to combust deposited coke on the catalyst. The amount of coke was determined based on the amount of CO_2 and CO formed during the combustion by FID-GC. The carbon balance of residual 1-MN and products (CO, CO_2, C_6H_6, $C_{10}H_8$, and coke) with respect to the fed 1-MN was $100 \pm 5\%$, which is acceptable within the experimental error. The 1-MN conversion, carbon-based yields, and product selectivities were calculated by the following equations, where the molecular formula represents the amount of each component.

$$\text{1-MNconversion}(\%) = ([\text{1-MN}]_{in} - [\text{1-MN}]_{out})/[\text{1-MN}]_{in} \times 100\% \quad (1)$$

$$C_{10}H_8\text{yield}(\%) = 10C_{10}H_8/(11[\text{1-MN}]_{in}) \times 100\% \quad (2)$$

$$C_6H_6\text{yield}(\%) = 6C_6H_6/(11[\text{1-MN}]_{in}) \times 100\% \quad (3)$$

$$\text{COyield}(\%) = \text{CO}/(11[\text{1-MN}]_{in}) \times 100\% \quad (4)$$

$$CO_2\text{yield}(\%) = CO_2/(11[\text{1-MN}]_{in}) \times 100\% \quad (5)$$

$$\text{Cokeyield}(\%) = \text{Coke}/(11[\text{1-MN}]_{in}) \times 100\% \quad (6)$$

$$(7)C_{10}H_8\text{selectivity}(\%) = C_{10}H_8\text{yield}/\text{1-MNconversion} \times 100\%$$

$$C_6H_6\text{selectivity}(\%) = C_6H_6\text{yield}/\text{1-MNconversion} \times 100\% \quad (8)$$

$$\text{COselectivity}(\%) = \text{COyield}/\text{1-MNconversion} \times 100\% \quad (9)$$

$$CO_2\text{selectivity}(\%) = CO_2\text{yield}/\text{1-MNconversion} \times 100\% \quad (10)$$

$$\text{Cokeselectivity}(\%) = \text{Cokeyield}/\text{1-MNconversion} \times 100\% \quad (11)$$

In all experiments, the amounts of toluene and CH_4 were much lower than those of other products (CO, CO_2, C_6H_6, $C_{10}H_8$, and coke) and were negligible in the selectivity calculation. The reaction conditions were adjusted on the basis of the purpose of the experiments such as kinetic studies, catalytic stability and so on. The reason of adjusting the reaction conditions was described in each experimental set. In typical tests, the reaction was carried out at 1123 K for 10 min using 1-MN/H_2O/N_2 = 1/12/87 with S/C = 1.1 and W/F = 0.25 g h mol^{-1} over 30 mg of catalyst. To investigate the influence of contact time (W/F), the catalyst weight and the total flow rate of reactants were changed to obtain W/F of 0.055–0.37 g h mol^{-1} (Supplementary material, Table S2). For kinetics measurement, the reaction was conducted at 1123 K over 50 mg of catalyst with W/F = 0.055 g h mol^{-1}. Furthermore, the formation rates of each products with time on stream was monitored at 1123 K for 0.5 h over 100 mg of catalyst using 1-MN/H_2O/N_2 = 1/12/87 with S/C = 1.1 and W/F = 0.37 g h mol^{-1} as well as 1-MN/H_2O/N_2 = 1/33/66 with S/C = 2.9 and W/F = 0.49 g h mol^{-1}.

2.3. Catalyst characterization

X-ray diffraction (XRD) patterns were recorded on a Rigaku Ultima IV diffractometer with Cu $K\alpha$ radiation (λ = 0.154 nm, 40 kV and 40 mA). The BET surface areas of the samples were measured by N_2 physical adsorption at 77 K on a Micromeritics Gemini 2360 analyzer. Scanning transmission electron microscopy (STEM) and energy dispersive X-ray (EDX) analysis were performed on a JEOL JEM-2100F electron microscope operated at an acceleration voltage of 200 kV. Samples for STEM were dispersed in ethanol by supersonic wave, and drops of suspensions were applied on a Mo grid coated with carbon film. The spot size of EDX analysis was ~1 nm.

H_2 chemisorption was carried out in a volumetric adsorption apparatus consisted of a high-vacuum glass system. The sample was pre-reduced with H_2/N_2 (30/30 mL min^{-1}) at 1073 K for 0.5 h in a fixed-bed reactor and a part of sample (~50 mg) was transferred to a cell for adsorption measurement. The sample was further in situ treated with H_2 (30 mL min^{-1}) at 773 K for 0.5 h, followed by evacuation at the same temperature for 0.5 h. The amount of H_2 adsorption was measured at ambient temperature. Hydrogen (99.99%) for volumetric adsorption was used as received. The dead volume of the apparatus was 63.5 cm^3, and the gas pressure at adsorption equilibrium was approximately 1.1 kPa.

H_2 temperature-programmed reduction (H_2-TPR) and O_2 temperature-programmed oxidation (O_2-TPO) were performed on a fixed-bed flow reactor connected to a TCD gas chromatograph. For H_2-TPR, the sample (~50 mg) was first pretreated with O_2 gas flow at 773 K for 0.5 h, followed by purging with high-purity N_2. After the sample was cooled to ambient temperature, a 5% H_2/Ar mixture (30 mL min^{-1}) was introduced into the reactor, and the effluent gas was passed through a frozen acetone trap to remove H_2O formed. The temperature was raised to 1273 K at a rate of 10 K min^{-1} and was maintained at 1273 K for 0.5 h. For O_2-TPO, the reduced sample (~50 mg) was first pretreated with H_2 gas flow at 773 K for 0.5 h, followed by purging with high-purity N_2. TPO was performed in 1% O_2/He mixture (30 mL min^{-1}) by raising the temperature from ambient temperature to 1073 K at a rate of 10 K min^{-1}. The reduction degrees of Ni and Cu were calculated based on the amount of O_2 consumption determined from TPO and the Cu°/Ni° ratio determined from XRD.

Diffuse reflectance infrared Fourier transform spectroscopy of CO adsorption (CO-FTIR) was performed on a Thermo Scientific Nicolet 6700 spectrometer using an IR cell with ZnSe windows. OMNIC software was used for data processing. The spectra were recorded at a resolution of 4 cm^{-1} using a liquid nitrogen-cooled MCT detector. The finely ground pre-reduced sample (~30 mg) was placed in a sample holder and was in situ treated in the DRIFT cell with 10% H_2/N_2 gas flow at 773 K for 0.5 h. After reduction treatment, the temperature was further held at 773 K for 0.5 h and the sample was purged with high-purity N_2. When the sample was cooled to ambient temperature under the N_2 flow, a reference spectrum of the pretreated sample was taken. Then pulses of 4% CO/He (1.5 μmol CO of one pulse) were repeatedly injected into the carrier stream and the spectrum was recorded after the adsorption saturation was reached. The IR spectrum of adsorbed CO was obtained by subtracting the spectrum of the pre-treated sample before CO adsorption.

The structure of coke deposited on the spent catalyst was analyzed by Raman spectroscopy. Raman spectra were recorded by using a Renishaw inVia Reflex Raman spectrometer from 630 to 1800 cm^{-1} at room temperature. The excitation source was the 532 nm line of Ar ion laser.

The amount of coke deposited on the spent catalyst was measured by thermogravimetric analysis (TG) on a Shimadzu TG-DTA-50 analyzer. Approximately 10 mg of spent catalyst was used, and the temperature was raised from 323 K to 1123 K at a rate of 10 K min^{-1} in air flow (50 mL min^{-1}).

The gasification of coke deposited on the spent catalyst was tested by temperature- programmed surface reaction with steam (H_2O-TPSR) using a fixed bed flow reaction system equipped with a Pfeiffer Vacuum Technology AG QMS200 mass spectrometer. 25 mg of the spent catalyst was loaded in the quartz tube reactor (i.d. 4 mm). The sample was pretreated with He flow at 573 K for 0.5 h. After cooling to 373 K, a 3% H_2O/He gas flow (~30 mL min^{-1}) was introduced into the reactor. H_2O was supplied by the gas stripping method at ~297 K. The temperature was increased to 1273 K by 10 K min^{-1} and held for 0.5 h. The signals with m/e = 28, 44, and 2 were used to monitor the CO, CO_2, and H_2 formed during TPSR.

3. Results and discussion

3.1. Catalyst characterization

The physicochemical properties of the LDHs-derived catalysts are summarized in Table 1. Some details on the structural characterization of the HTlcs precursors and their calcined and reduced products were reported previously [27]. The XRD patterns of the as-synthesized precursors clearly revealed the formation of pure HTlcs at the whole composition range investigated (Supplementary material, Fig. S1). Upon calcination at 1073 K, the HTlcs were converted to Mg(Ni, Cu, Al)O solid solutions together with minor $CuAl_2O_4$ spinel at Cu/Ni ≥0.5 (Supplementary material, Fig. S2). After reduction with H_2 at 1073 K, both Ni^{2+} and Cu^{2+} were reduced

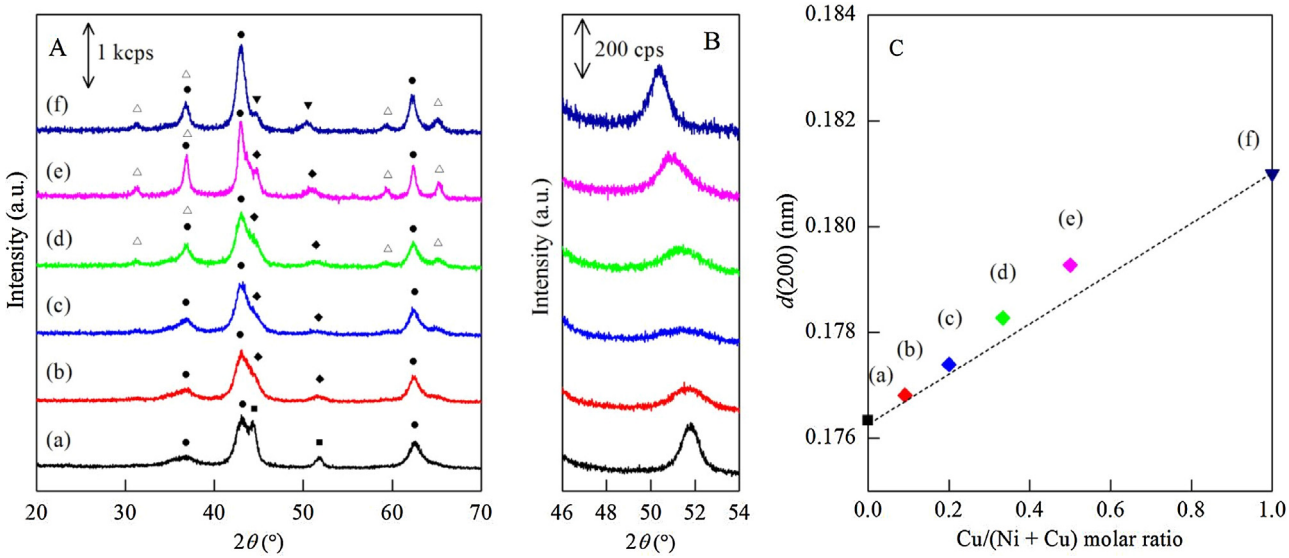

Fig. 1. (A) XRD patterns of the catalysts after reduction at 1073 K: (a) Ni/Mg/Al [27], (b) Ni-Cu/Mg/Al (Cu/Ni = 0.1), (c) Ni-Cu/Mg/Al (Cu/Ni = 0.25) [27], (d) Ni-Cu/Mg/Al (Cu/Ni = 0.5), (e) Ni-Cu/Mg/Al (Cu/Ni = 1.0), and (f) Cu/Mg/Al [27]. Crystalline phases: (●) MgO-like solid solution, (■) Ni metal, (♦) Ni-Cu alloy, (▼) Cu metal, (△) spinel. (B) 46–54° regional XRD patterns. (C) Dependence of *d*(200) spacing as a function of Cu/(Ni + Cu) molar ratio in the catalyst. The dot line represents theoretical Vegard's law behavior based on Ni and Cu metals.

from Mg(Ni, Cu, Al)O to form Ni-Cu alloys. The formation of uniform Ni-Cu alloy nanoparticles has been confirmed by the XRD and STEM-EDX measurements. The XRD patterns (Fig. 1A and B) showed that the diffractions peaks of Ni metal became broader and gradually shifted to lower angles with increasing the Cu/Ni ratio, suggesting the formation of small-sized Ni-Cu alloy nanoparticles. The STEM images (Fig. 2) revealed that the particles were homogeneously distributed on the surface with a relatively narrow size distribution and the mean particle size ($\sum n_i d_i^3 / \sum n_i d_i^2$) decreased with the increase of Cu/Ni ratio (ca. 5–7 nm). The Cu°/Ni° ratio in the particles determined by EDX was 0.10–0.15, 0.28–0.36, and 0.72–0.87 for Ni-Cu/Mg/Al (Cu/Ni = 0.1, 0.25, 0.5), respectively (Supplementary material, Fig. S3), which are well consistent with the values calculated from the *d*(200) spacings by Vegard's law (Fig. 1C, Table 1), demonstrating the uniform composition of the Ni-Cu alloy nanoparticles. The Cu°/Ni° ratio of Ni-Cu alloys was higher than the Cu/Ni ratio in the catalyst, which could be attributed to the higher reducibility of Cu than Ni as indicated by the H_2-TPR measurement (Supplementary material, Fig. S4 and [27]). It is noted that the dispersion of Ni-Cu alloys estimated from H_2 chemisorption and O_2-TPO (Supplementary material, Fig. S5) was smaller than that calculated from STEM and the difference became more significant with increasing the Cu/Ni ratio. This difference can be attributed to the suppression of H_2 adsorption by the presence of Cu on the particle surface [27]. Based on the dispersions estimated from H_2 adsorption and STEM, the alloy surface composition was calculated. The surface Cu°/Ni° ratio was much higher than the bulk Cu°/Ni° ratio, suggesting that Cu atoms were enriched on the alloy surface, in agreement with previous reports [30–32]. The Cu surface enrichment might be related to the lower surface energy of Cu compared with Ni [33].

To get more information on the surface state of the Ni-Cu alloy nanoparticles, FTIR measurement was carried out using CO as the molecule probe. Fig. 3 shows the FTIR spectra of absorbed CO on the reduced catalysts. The Ni/Mg/Al catalyst exhibited two strong bands at ~2069 and 1945 cm^{-1}, which could be assigned to linear and bridged CO on Ni metal, respectively [21], whereas the Cu/Mg/Al catalyst showed only one weak band at ~2103 cm^{-1} attributable to linear CO on Cu metal [34]. For the Ni-Cu/Mg/Al catalysts, two bands at the ranges of 2096–2102 and 2003–2019 cm^{-1} were observed. The former, which was similar to that observed on the Cu/Mg/Al catalyst, was ascribed to linear CO on the Cu metal atoms in the alloy surface, whereas the latter might be mainly due to linear CO on the Ni metal atoms of the alloys. No significant bridged CO band on Ni metal was found. It is noted that the linear CO on Ni metal was significantly shifted to 2019 cm^{-1} by 46 cm^{-1} as the Cu/Ni ratio rose from 0 to 0.1 and its intensity increased remarkably; the band continued to move toward lower wavenumbers with further increasing the Cu/Ni ratio, but its intensity gradually decreased. The intensity change of the linear CO on Ni metal was consistent with the tendency of H_2 chemisorption (Table 1). Concerning the red-shift of the linear CO on Ni metal, one consideration is due to the ligand effect. However, since the electronegativity of Cu metal (1.90) is quite similar to that of Ni metal (1.91) [35], the electron transfer between Cu and Ni metal atoms would be limited, which was in part supported by that the linear CO on Cu metal was located at almost the same wavenumber. Sona-Moto et al. [36] also pointed out in their work on CO adsorption on Ni-Cu/SiO_2 that the ligand effect had little effect on the adsorption of CO on Ni. One possible explanation for the CO red-shift is the particle size effect. As shown in Table 1, the particle size decreased from 10.8 to 5.1 nm as the Cu/Ni ratio increased from 0 to 1.0. With the decrease of particle size, the fraction of face atoms would decrease and those of corner atoms and edge atoms would increase. Since the corner atoms and edge atoms are more coordinately unsaturated, this might cause a higher degree of back-donation of electrons into the antibonding π^* orbital of CO, weakening the strength of C—O bond and resulting in a low-wavenumber shift [37,38]. On the other hand, the absence of the bridged CO band can be interpreted as due to the geometric effect, i.e., dilution of the Ni surface by Cu, which decreased the number of two neighbouring Ni atoms and as a result the intensity of bridged CO. We have tried to calculate the surface Cu°/Ni° ratio from the relative intensities of CO bands on Cu and Ni atoms (Supplementary material, Table S3). However, owing to the weak reversible chemisorption and uncertain adsorption stoichiometry of CO on metallic Cu surface [39], it was difficult

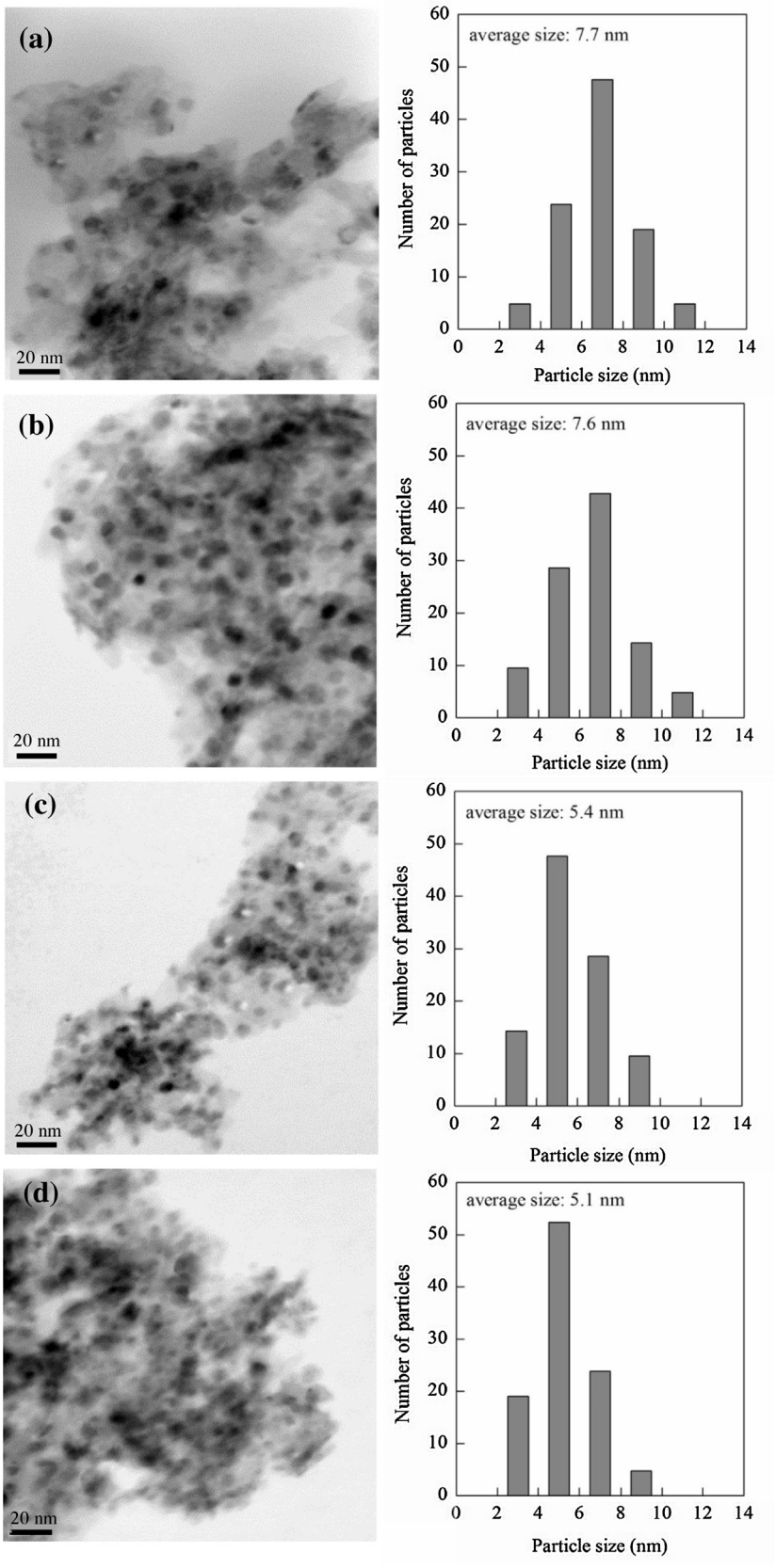

Fig. 2. STEM images and particle size distributions of the reduced catalysts: (a) Ni-Cu/Mg/Al (Cu/Ni = 0.1), (b) Ni-Cu/Mg/Al (Cu/Ni = 0.25), (c) Ni-Cu/Mg/Al (Cu/Ni = 0.5), and (d) Ni-Cu/Mg/Al (Cu/Ni = 1.0).

Table 1
Physicochemical property of the reduced catalysts.

Catalyst	Content ($mmol\ g_{cat}^{-1}$)		Cu°/Ni° of alloy particles[a]	Particle size[b] (nm)	O_2 consumption[c] ($mmol\ g_{cat}^{-1}$)	Reduction degree[d] (%)		H_2 adsorption[e] ($\mu mol\ g_{cat}^{-1}$)	Dispersion (%)		$Cu^{\circ}{}_s/Ni^{\circ}{}_s$ of alloy surface[h]
	Ni	Cu				Ni	Cu		H_2 adsorption[f]	STEM[g]	
Ni/Mg/Al [27]	2.04	0	0	10.8	0.55	54	–	42.5	7.7	9.0	–
Ni-Cu/Mg/Al (Cu/Ni = 0.1)	2.04	0.20	0.13	7.7	0.88	76	99	93.2	10.6	12.5	0.18
Ni-Cu/Mg/Al (Cu/Ni = 0.25) [27]	2.04	0.50	0.33	7.6	0.96	71	94	64.6	6.7	13.2	0.85
Ni-Cu/Mg/Al (Cu/Ni = 0.5)	2.04	1.02	0.79	5.4	1.08	59	94	56.9	5.3	17.2	2.3
Ni-Cu/Mg/Al (Cu/Ni = 1.0)	2.04	2.04	1.98	5.1	1.53	50	99	49.5	3.2	17.7	4.5
Cu/Mg/Al [27]	0	2.04	–	4.5	0.95	–	93	3.2	0.3	–	–

[a] Calculated from the $d(200)$ spacing from XRD by the Vegard's law: $d_{Ni\text{-}Cu} = Ni/(Ni+Cu) \times d_{Ni} + Cu/(Ni+Cu) \times d_{Cu}$, where d_{Ni} and d_{Cu} are 0.1762 nm (JCPDS 01-070-1849) and 0.1808 nm (JCPDS 04-0836), respectively.
[b] Determined by STEM according to $\sum n_i d_i^3 / \sum n_i d_i^2$.
[c] Measured by TPO on the reduced catalysts.
[d] Calculated on the basis of O_2 consumption in O_2-TPO and Cu°/Ni° ratio from XRD, assuming that $Ni^{\circ} + 1/2O_2 \rightarrow NiO$ and $Cu^{\circ} + 1/2O_2 \rightarrow CuO$.
[e] Measured by H_2 adsorption at room temperature.
[f] Calculated by the equation: Dispersion (%) = (2 × H_2 adsorption)/(O_2 consumption/2) × 100%.
[g] Calculated by the equation: Dispersion (%) = $A_{Ni\text{-}Cu}$/particle size (nm) × 100%, where $A_{Ni\text{-}Cu} = A_{Ni} \times (Ni/(Ni+Cu)) + A_{Cu} \times (Cu/(Ni+Cu))$, $A_{Ni} = 0.971$ [28], $A_{Cu} = 1.1$ [29].
[h] Calculated using the equation: (Dispersion (STEM) − Dispersion (H_2 adsorption))/(Dispersion (H_2 adsorption)).

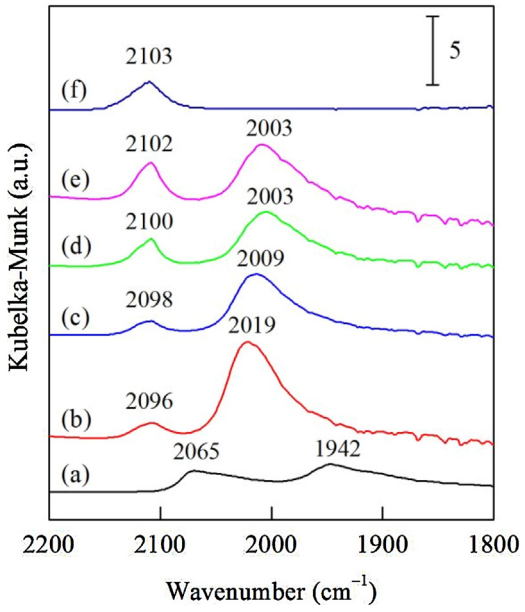

Fig. 3. FTIR spectra of absorbed CO on the reduced catalysts: (a) Ni/Mg/Al, (b) Ni-Cu/Mg/Al (Cu/Ni = 0.1), (c) Ni-Cu/Mg/Al (Cu/Ni = 0.25), (d) Ni-Cu/Mg/Al (Cu/Ni = 0.5), (e) Ni-Cu/Mg/Al (Cu/Ni = 1.0), and (f) Cu/Mg/Al.

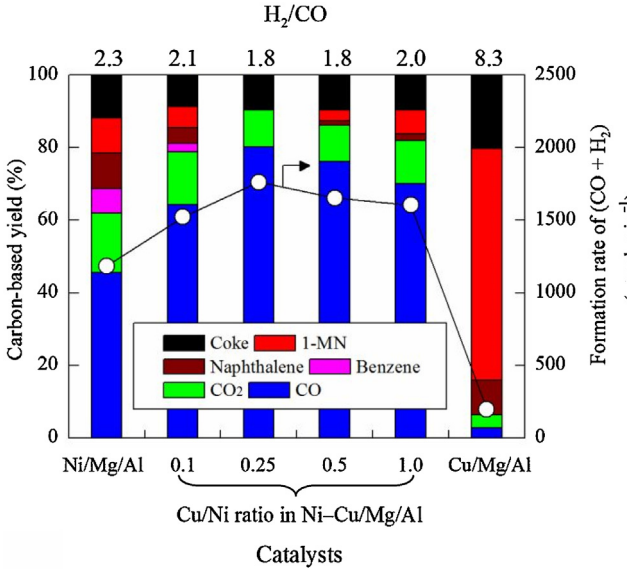

Fig. 4. Catalytic activities of Ni-Cu/Mg/Al catalysts in the steam reforming of 1-methyl naphthalene. Reaction conditions: 1123 K, 1-MN/H_2O/N_2 = 1/12/87, S/C = 1.1, W/F = 0.25 g h mol^{-1}, catalyst 30 mg, reaction time 10 min; reduction, H_2/N_2 = 30/30 mL min^{-1} at 1073 K for 0.5 h.

to determine the value properly. Nevertheless, from the significant decrease of bridged CO band at Cu/Ni ≤0.25, where the Cu°/Ni° ratio in the alloy was rather low, it is reasonable to consider that Cu was enriched on the alloy surface, which in part supported the result of H_2 chemisorption.

3.2. Catalytic performance in the steam reforming of 1-MN

3.2.1. Effect of Cu/Ni ratio

Fig. 4 shows the catalytic activity of Ni-Cu/Mg/Al catalysts in the steam reforming of 1-MN. The reaction was carried out at 1123 K with 1-MN/H_2O/N_2 = 1/12/87, S/C = 1.1, and W/F = 0.25 g h mol^{-1} over 30 mg of catalyst. The purpose of these experiments is to optimize the molar ratio of Cu/Ni in Ni-Cu/Mg/Al catalysts and the

reaction conditions such as *W/F* were adjusted on the basis that 1-MN conversion did not reach 100% on the catalysts other than that with the optimized Cu/Ni. Since the catalyst gradually lost its activity with time on stream (Supplementary material, Fig. S6), the activity was evaluated for 10 min and the carbon-based yield was calculated based on the average value (the same below). In addition to the deposited coke on the catalyst, the products mainly involved H_2, CO, CO_2, together with small amounts of naphthalene and benzene. The formation of naphthalene and benzene was probably arising from the steam dealkylation and ring opening of 1-MN [40]. CH_4 and other light hydrocarbons were negligible. It is found that the activity of the Ni-Cu/Mg/Al catalysts exhibited a volcano-type dependence on the Cu/Ni ratio. As the Cu/Ni ratio increased from 0 to 0.25, the yields of residual 1-MN, naphthalene, and benzene gradually decreased and became almost zero at Cu/Ni = 0.25. Meanwhile, the formation rate of syngas ($CO + H_2$) increased and reached a maximum at Cu/Ni = 0.25. As the Cu/Ni ratio exceeded 0.25, the yields of residual 1-MN and naphthalene increased and the formation rate of syngas decreased. On the Cu/Mg/Al catalyst, the yield of residual 1-MN was rather high, and the formation rate of syngas was quite low, indicating that copper only was not active enough for the steam reforming of 1-MN under the present reaction conditions. The poor activity of copper for catalytic reforming of hydrocarbons has been documented [41]. Compared to the case of the steam reforming of biomass tar, the effect of Cu/Ni on the catalytic performance was more significant in the steam reforming of 1-MN because of lower reactivity of 1-MN [27]. It was verified that the best catalyst was Ni-Cu/Mg/Al (Cu/Ni = 0.25). It is noted that the order of catalyst activity was somewhat different with the tendency of H_2 adsorption on the catalyst, although the amount of H_2 adsorption was increased by the Ni-Cu alloying. Thus, the catalyst activity cannot be simply related to the increase of Ni metal active sites. To get full image on the promoting effect of Ni-Cu alloying, the comparison of the catalytic behaviors of Ni-Cu/Mg/Al (Cu/Ni = 0.25) and Ni/Mg/Al catalysts was further carried out in the steam reforming of 1-MN under different reaction conditions, although it is not easy in the case of the steam reforming of biomass tar.

3.2.2. Effect of contact time

Fig. 5 shows the changes of 1-MN conversion and product selectivities with contact time, expressed as the ratio of catalyst weight to the total flow rate (*W/F*), on the two catalysts. The detailed results are summarized in Table S2 (Supplementary material). In these experiments, we adjusted *W/F* by changing the catalyst loading and the flow rate because stable flow rate of 1-MN was available in limited range due to high boiling point of 1-MN. Generally, 1-MN conversion increased with increasing the *W/F*, leading to higher CO selectivity and gas yield ($CO + CO_2$) as well as lower selectivities toward naphthalene and benzene. The Ni-Cu/Mg/Al (Cu/Ni = 0.25) catalyst always showed higher 1-MN conversion than the Ni/Mg/Al catalyst at the *W/F* values investigated. Particularly, full conversion of 1-MN was obtained on the Ni-Cu/Mg/Al (Cu/Ni = 0.25) catalyst at $W/F \geq 0.25$ g h mol^{-1}, and no formation of naphthalene and benzene was observed. Based on the 1-MN conversion at $W/F = 0.055$ g h mol^{-1} and the amount of H_2 adsorption, the turnover frequency (TOF) of 1-MN was calculated to be 0.16 and 0.13 s^{-1} for Ni/Mg/Al and Ni-Cu/Mg/Al (Cu/Ni = 0.25), respectively. Correspondingly, the TOF of $CO + CO_2$ formation was calculated to be 1.02 and 0.87 s^{-1}, respectively. The TOF values of the Ni-Cu/Mg/Al (Cu/Ni = 0.25) were slightly lower than those of the Ni/Mg/Al catalyst. This is probably due to the surface modification of Ni with less active Cu. It should be noted that the total selectivity of $CO + CO_2$ was higher on Ni-Cu/Mg/Al (Cu/Ni = 0.25) than on Ni/Mg/Al, and the selectivities of benzene, naphthalene, and coke were lower on the former than on the latter. This implies that the gasification of carbonaceous species was promoted on the Ni-Cu alloy particles, and the side reactions such as cracking, ring opening, and/or steam dealkylation of 1-MN were suppressed.

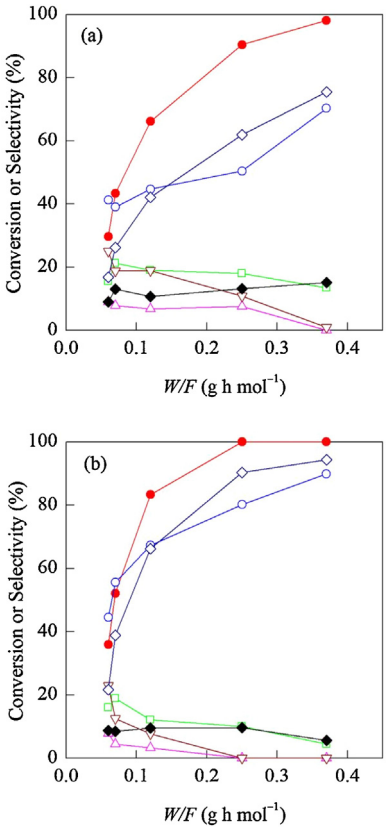

Fig. 5. Effect of contact time (*W/F*) on the conversion and product selectivities over (a) Ni/Mg/Al and (b) Ni-Cu/Mg/Al (Cu/Ni = 0.25): (●) 1-MN conversion, (○) CO selectivity, (□) CO_2 selectivity, (▽) naphthalene selectivity, (△) benzene selectivity, (♦) coke selectivity, (◇) ($CO + CO_2$) gas yield. Reaction conditions: 1123 K, 1-MN/H_2O/N_2 = 1/12/87, S/C = 1.1, *W/F* = 0.055-0.37 g h mol^{-1}, catalyst 30–150 mg, reaction time 10 min; reduction, H_2/N_2 = 30/30 mL min^{-1} at 1073 K for 0.5 h.

3.2.3. Effect of reactant partial pressure

The effect of 1-MN and steam partial pressures on the catalyst activity was further investigated. Here it is essential that the 1-MN conversion should be clearly lower than 100% because the change of the partial pressures of 1-MN and water should be minimized for this investigation, and then we realized the lower 1-MN conversion by adopting the reaction conditions with lower *W/F* based on the result of the *W/F* dependence (Fig. 5). As a result, the reaction conditions at 1123 K with $W/F = 0.055$ g h mol^{-1} over 50 mg of catalyst were selected, and the S/C ratio was changed in the range between 0.8 and 1.4 under the present conditions. The obtained results are shown in Table 2 and the changes of 1-MN reaction rate and $CO + CO_2$ formation rate against the reactant partial pressures are plotted in Fig. 6. Generally, the 1-MN conversion decreased with increasing the 1-MN partial pressure or decreasing the steam partial pressure. H_2, CO, and CO_2 were the main products, and only a small amount of benzene and naphthalene were formed. In most cases, the 1-MN reaction rate and $CO + CO_2$ formation rate were higher on the Ni-Cu/Mg/Al (Cu/Ni = 0.25) catalyst than on the Ni/Mg/Al catalyst except for at high steam partial pressure. When the steam partial pressure was kept at 12.34% and the 1-MN partial pressure varied from 0.78% to 1.30% (Fig. 6a), the 1-MN reaction rate and $CO + CO_2$ formation rate on both catalysts increased only slightly. The reaction order of 1-MN was about 0.2 for both catalysts, and that of $CO + CO_2$ formation rate was approximately 0.1 and 0 for Ni/Mg/Al and Ni-Cu/Mg/Al (Cu/Ni = 0.25), respectively. The

Table 2
Effect of partial pressures of 1-methyl naphthalene and steam on catalytic activity over Ni/Mg/Al and Ni-Cu/Mg/Al (Cu/Ni = 0.25) catalysts.

Catalysts	Partial pressure (%)			Conversion (%)	Flow rate (μmol min^{-1})					Reaction rate of 1-MN[a] (mmol g^{-1} h^{-1})	Formation rate of (CO+ CO_2)[b] (mmol g^{-1} h^{-1})
	1-MN	H_2O	N_2		H_2	CO	CO_2	Benzene	Naphthalene		
Ni/Mg/Al	0.78	12.34	86.88	41.7	578	259	69	2	3	59.1	394
	1.04	12.34	86.62	33.6	659	241	111	2	3	63.5	422
	1.30	12.34	86.36	27.6	614	257	89	2	3	65.2	415
	1.04	8.23	90.73	25.4	482	205	47	2	3	48.0	302
	1.04	16.44	82.52	46.5	478	304	151	3	4	87.9	546
Ni-Cu/Mg/Al (Cu/Ni = 0.25)	0.78	12.34	86.88	54.9	402	357	99	2	3	77.8	547
	1.04	12.34	86.62	44.7	925	372	86	2	4	84.5	550
	1.30	12.34	86.36	35.9	792	342	113	2	4	84.8	546
	1.04	8.23	90.73	38.6	576	362	97	2	3	73.0	551
	1.04	16.44	82.52	47.0	815	300	138	2	4	88.9	526

Other reaction conditions: 1123 K, S/C = 0.8–1.4, W/F = 0.055 g h mol^{-1}, catalyst 50 mg; reduction, H_2/N_2 = 30/30 mL min^{-1} at 1073 K for 0.5 h.
[a] Calculated by 1-MN partial pressure × 1-MN conversion/(W/F).
[b] Calculated by flow rates of (CO + CO_2)/catalyst weight.

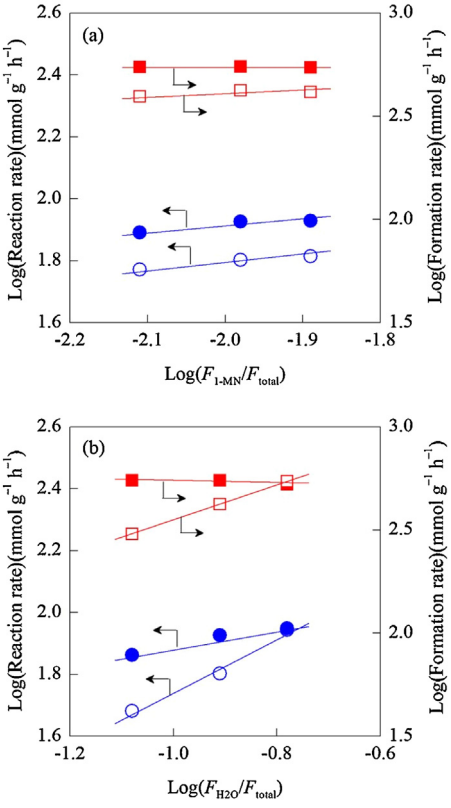

Fig. 6. Effect of (a) 1-MN and (b) steam partial pressure on the catalytic activity over Ni/Mg/Al (open) and Ni-Cu/Mg/Al (Cu/Ni = 0.25) (solid): (○, ●) 1-MN reaction rate, (□, ■) formation rate of CO + CO_2. Reaction conditions: 1123 K, S/C = 0.8 ~ 1.4, W/F = 0.055 g h mol^{-1}, catalyst 50 mg, reaction time 10 min; reduction, H_2/N_2 = 30/30 mL min^{-1}, 1073 K, 0.5 h.

low reaction order of 1-MN may suggest that 1-MN was strongly adsorbed on the catalyst and the coverage of 1-MN was almost saturated, and the similar reaction order of 1-MN on both catalysts indicates that the adsorption of 1-MN was not influenced by the formation of Ni-Cu alloys. When the 1-MN partial pressure was kept at 1.04% and the steam partial pressure varied from 8.23% to 16.44% (Fig. 6b), great differences between the two catalysts were observed. On the Ni/Mg/Al catalyst, the 1-MN reaction rate and CO + CO_2 formation rate increased significantly with increasing the steam partial pressure, the reaction orders being about 0.9, suggesting that the catalyst activity was strongly dependent on the steam partial pressure. This may also suggest that steam was weakly adsorbed on the Ni metal particles on Ni/Mg/Al. On the other hand, on the Ni-Cu/Mg/Al (Cu/Ni = 0.25) catalyst, the 1-MN reaction rate increased only slightly with increasing the steam partial pressure, and the CO + CO_2 formation rate tended to decrease, the reaction orders being about 0.3 and −0.1, respectively. The reaction order of 1-MN with respect to the steam partial pressure was lower on the Ni-Cu/Mg/Al (Cu/Ni = 0.25) catalyst than on the Ni/Mg/Al catalyst, suggesting that steam was more strongly adsorbed on the alloy catalyst. This is in part supported by the O_2-TPO result (Supplementary material, Fig. S5 and [27]) that the Ni-Cu alloys had higher oxygen affinity than the Ni metal. It can be inferred from this result that the adsorption of steam was significantly promoted by the Ni-Cu alloying and the coverage of H_2O was also increased in spite of high coverage of 1-MN. One possible interpretation is that the adsorption of 1-MN on Ni atom was saturated and Cu atom in the case of Ni-Cu alloy surface may play a role as the vacant site for H_2O adsorption. Steam activation is an important step for steam reforming of hydrocarbons and it is widely accepted that H_2O reacts with surface Ni atoms, providing gaseous hydrogen and adsorbed oxygen; adsorbed oxygen further reacts with carbonaceous species on Ni surface, yielding gaseous CO and H_2 [1]. Accordingly, we think that the small Ni-Cu alloy particles could promote the dissociative adsorption of steam to form more adsorbed oxygen species, which enhanced the gasification of carbonaceous species, leading to higher activity and lower coke deposition.

3.2.4. Activity with time on stream

The effect of time on stream was investigated for the evaluation of the catalyst stability. As is known, catalyst deactivation can be caused by coke deposition, aggregation of active metal particles, and so on. An important point is that the coke deposition can be due to both the decomposition of hydrocarbon substrates and the disproportionation of the produced CO. This means that the catalyst stability had better be evaluated at high conversion level where the high partial pressure of the hydrocarbon substrates is obtained at the catalyst bed inlet and the high partial pressure of CO is obtained at the catalyst bed outlet. Therefore, we selected the reaction conditions at high W/F such as 0.37 g h mol^{-1} on the basis of the result in Fig. 5. Fig. 7 shows the formation rates of gaseous products and CO + CO_2 gas yield with time on stream over the two catalysts. Under the conditions of S/C = 1.1 and W/F = 0.37 g h mol^{-1} (Fig. 7A), the Ni/Mg/Al catalyst was quickly deactivated after 15 min of reaction, while the Ni-Cu/Mg/Al (Cu/Ni = 0.25) catalyst showed a relatively stable activ-

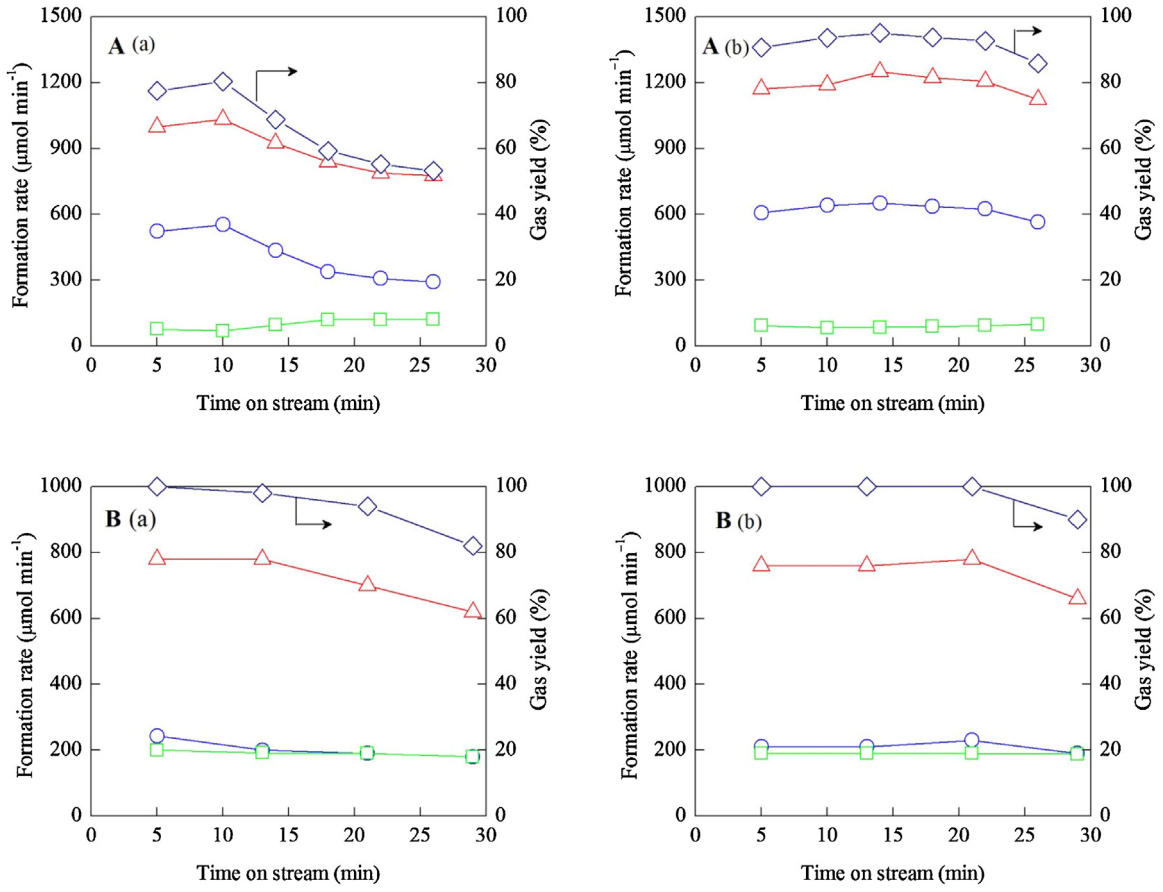

Fig. 7. Formation rates of gaseous products and carbon-based gas yield with time on stream over (a) Ni/Mg/Al and (b) Ni-Cu/Mg/Al (Cu/Ni = 0.25): (○) CO, (□) CO_2, (△) H_2, (◊) (CO + CO_2) gas yield. Reaction conditions: (A) 1-MN/H_2O/N_2 = 1/12/87 (1-MN flow rate 70 μmol min^{-1}), S/C = 1.1, *W/F* = 0.37 g h mol^{-1}, catalyst 150 mg; (B) 1-MN/H_2O/N_2 = 1/33/66 (1-MN flow rate 34 μmol min^{-1}), S/C = 2.9, *W/F* = 0.49 g h mol^{-1}, catalyst 100 mg; other conditions, 1123 K, reduction, H_2/N_2 = 30/30 mL min^{-1}, 1073 K, 0.5 h.

ity, although the activity was slightly decreased after 25 min of reaction. During the time on stream investigated, the activity of Ni-Cu/Mg/Al (Cu/Ni = 0.25) was always higher than that of Ni/Mg/Al.

The S/C ratio significantly influences the catalytic activity and stability as well as coke deposition. The steam reforming of hydrocarbons was conventionally carried out at higher S/C than 1. Therefore, we also evaluated the catalytic performance at S/C = 2.9. When increasing the S/C to 2.9 and *W/F* to 0.49 g h mol^{-1} for the high conversion level (Fig. 7B), the carbon-based CO + CO_2 yield on both catalysts was kept above 80%, the average gas yield being about 93.5% and 97.5%, respectively; under this condition, the Ni-Cu/Mg/Al (Cu/Ni = 0.25) catalyst also exhibited higher activity and stability than the Ni/Mg/Al catalyst, demonstrating the promoting effect of Ni-Cu alloying. Nevertheless, it is also noted that both catalysts were catalytically less stable in the steam reforming of 1-MN than in the steam reforming of biomass tar [27]. This can be due to that coke was formed more easily from 1-MN than from the biomass tar. In the steam reforming of biomass tar, biomass tar was derived from the pyrolysis of cedar wood at 923 K, which mainly consists of single ring aromatics such as benzene and toluene etc, while in this study poly-aromatic 1-MN was used, which induces coke deposition more easily than single ring aromatics.

It is well known that coke deposition and agglomeration of metal particles are the two main causes for the catalyst deactivation in catalytic reforming of hydrocarbons [42]. In addition, oxidation of metal and/or structural change may also occur [19]. To check the coke deposition, metal particle size, and catalyst structure, the spent catalysts after the reaction (Fig. 7B) were characterized by XRD, STEM, Raman, and TG analysis. The XRD result (Fig. 8A) clearly showed the agglomeration of Ni metal particles on the spent Ni/Mg/Al catalyst; the size of Ni metal particles was calculated by the Scherrer equation to be ~15.4 nm, much larger than the freshly reduced one (8.5 nm) [25]. For the spent Ni-Cu/Mg/Al catalyst, the formation of Ni-Cu alloy was also confirmed by XRD. The average composition of Cu°/Ni° was calculated by the Vegard's law to be about 0.33, similar to the reduced one, suggesting little change of the alloy composition; nevertheless, the diffraction peak of Ni-Cu alloy became strong. The size of Ni-Cu alloy particles determined by STEM (Fig. 8B) was ~9.2 nm, slightly larger than the freshly reduced one. Raman spectra (Fig. 8C) showed the presence of two bands at ~1350 and 1595 cm^{-1}, which could be assigned to the defect (D band) and graphitic carbon (G band), respectively [43]. No great differences in the peak intensity and position were observed, suggesting that the deposited coke on both catalysts had a similar structure. It is known that hydrocarbon decomposition ($C_xH_y \rightarrow xC + y/2H_2$) and CO disproportionation ($2CO \rightarrow C + CO_2$) are the two main routes for the coke deposition [44]. The former usually occurs at the catalyst bed inlet, while the latter is favorable at the catalyst bed outlet. Thus, the amount of deposited coke on the catalyst bed inlet and outlet was separately measured by TG analysis (Supplementary material, Fig. S7 and Table S4). It was 115.3 (inlet) and 15.4 (outlet) mg-C g_{cat}^{-1} for the Ni/Mg/Al catalyst, and 44.8 (inlet) and 9.1 (outlet) mg-C g_{cat}^{-1} for the Ni-Cu/Mg/Al (Cu/Ni = 0.25) catalyst, respectively. Obviously, the amount of deposited coke at the catalyst bed inlet was much higher than that at the catalyst bed outlet, suggesting that the

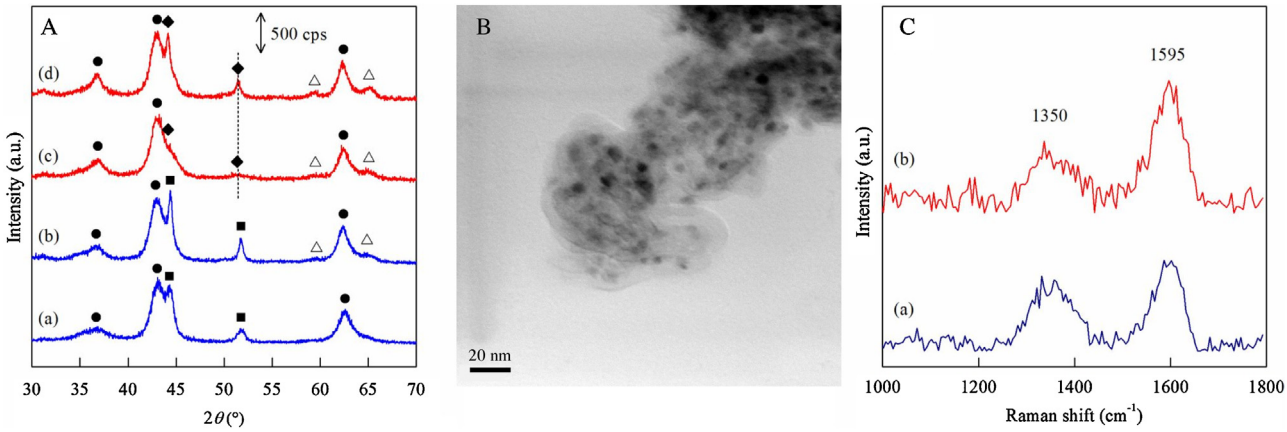

Fig. 8. (A) XRD patterns of (a, b) Ni/Mg/Al and (c, d) Ni-Cu/Mg/Al (Cu/Ni = 0.25) catalysts after reduction (a, c) and after reaction (b, d) (Fig. 7B). Crystalline phases: (●) MgO-like solid solution, (■) Ni metal, (♦) Ni-Cu alloy, (△) spinel. (B) STEM image of the Ni-Cu/Mg/Al (Cu/Ni = 0.25) catalyst after reaction (Fig. 7B). (C) Raman spectra of deposited coke on (a) Ni/Mg/Al and (b) Ni-Cu/Mg/Al (Cu/Ni = 0.25) after reaction (Fig. 7B).

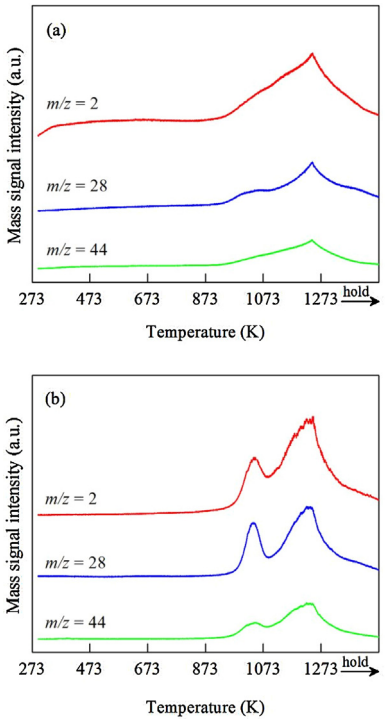

Fig. 9. H_2O-TPSR of deposited coke on the catalysts after reaction (Fig. 7B): (a) Ni/Mg/Al and (b) Ni-Cu/Mg/Al (Cu/Ni = 0.25). Measurement conditions: spent catalyst, 25 mg; H_2O/He = 3/97, 10 K min^{-1}, from 373 to 1273 K and hold at 1273 K for 0.5 h.

coke deposition was mainly due to the hydrocarbon decomposition. This is expected, since hydrocarbon decomposition is endothermic and favorable at high temperature while it is the opposite for CO disproportionation. It should be noted that the coke deposition on the inlet catalyst was about 1/3 times less for Ni-Cu/Mg/Al (Cu/Ni = 0.25) than for Ni/Mg/Al, indicating better coke resistance of the Ni-Cu alloy catalyst.

The gasification behavior of coke deposited on the spent catalyst was further studied by temperature-programmed surface reaction with steam (H_2O-TPSR) over the inlet catalyst. The possible gasification products including CO, CO_2, and H_2 were monitored by mass spectroscopy. As shown in Fig. 9, the signals due to H_2, CO, and CO_2 started to appear above ~953 K, corresponding to the steam gasification of coke ($C + H_2O \rightarrow CO + H_2$ and $C + 2H_2O \rightarrow CO_2 + 2H_2$). Two peaks at ~1036 K and >1223 K were observed. No significant temperature-shift of the peaks between the two catalysts was found; nevertheless, the peak intensity particularly for the low-temperature peak was much higher on the Ni-Cu/Mg/Al (Cu/Ni = 0.25) catalyst than on the Ni/Mg/Al catalyst. The amount of gasified coke was calculated by integrating the peak areas of CO and CO_2. It was ~2.4 mmol-C g_{cat}^{-1} for Ni/Mg/Al, corresponding to only 1/4 of the deposited coke (9.6 mmol-C g_{cat}^{-1}), while it was ~3.7 mmol-C g_{cat}^{-1} for Ni-Cu/Mg/Al (Cu/Ni = 0.25), nearly identical to the amount of deposited coke, suggesting that the deposited coke was almost completely gasified with steam below 1223 K. This result indicates that the steam gasification of coke was promoted on the Ni-Cu alloy nanoparticles.

According to the literature [45], the process of coke deposition on the nickel surface can be briefly described as follows. Hydrocarbons dissociate on the nickel surface to produce carbon species. The carbon may be gasified, may dissolve the nickel particle, or may encapsulate the surface. The dissolved carbon diffuses through the nickel or via nickel carbide to nucleate and precipitate at the rear of the particle, leading to the formation of a carbon whisker. When the rate of carbon diffusion through the particle is slower than that of carbon formation at the surface, carbon builds up at the surface and encapsulates the particle, leading to encapsulating carbons. Typically, coke deposition occurs easily on large Ni particles because it requires sufficiently large ensemble of Ni metal atoms for carbon growth. As shown above, the formation of Ni-Cu alloy nanoparticles on the Ni-Cu/Mg/Al (Cu/Ni = 0.25) catalyst effectively suppressed the coke deposition, and this can be considered from several aspects. Firstly, the small Ni-Cu alloy particles might promote the steam activation and as a result enhance the coke gasification, as indicated from the results of O_2-TPO, kinetics, and H_2O-TPSR, leading to less carbon species on the particle surface. Secondly, alloying Ni with Cu decreased the particle size, which would reduce the large ensemble of Ni metal atoms for carbon growth. It has been well reported that coke deposition is strongly influenced by the particle size and small particles have higher coke resistance [46,47]. Thirdly, as indicated from the results of H_2 chemisorption and CO-FTIR, Cu metal atoms tended to be enriched on the particle surface. This surface modification would further eliminate the large ensemble of Ni metal atoms responsible for generation of carbon filaments. Moreover, owing to the lower

surface energy of Cu compared with Ni, the surface Cu atoms might preferably occupy at steps and edges of the particle surface which are the nucleation sites for carbon formation [33,48].

4. Conclusion

The Ni-Cu alloy catalysts prepared from the Ni-Cu-Mg-Al HTlcs (Cu/Ni = 0.1–1.0) were well-dispersed and composition-uniform. The particle size was decreased with increasing the Cu/Ni ratio, and Cu had a tendency to be enriched on the particle surface. The isomorphous incorporation of Ni^{2+} and Cu^{2+} in the HTlcs and the resulted solid solution is important for the formation of uniform Ni-Cu alloy nanoparticles. In the steam reforming of 1-MN, the catalysts showed a volcano-type dependence of activity on the Cu/Ni ratio; the highest reforming activity and lower yields of byproducts including benzene, naphthalene, and coke were obtained on the Ni-Cu/Mg/Al (Cu/Ni = 0.25) catalyst. Compared to Ni/Mg/Al, Ni-Cu/Mg/Al (Cu/Ni = 0.25) showed higher selectivity of $CO + CO_2$ and lower selectivities of benzene, naphthalene, and coke, suggesting that the gasification of carbonaceous species was promoted and the side reactions were suppressed on the Ni-Cu alloy nanoparticles. The kinetic study showed that the reaction order of 1-MN with respect to the 1-MN partial pressure was low and similar for the Ni and Ni-Cu catalysts; on the other hand, the reaction order of 1-MN with respect to the steam partial pressure was lower on the Ni-Cu catalyst than on the Ni catalyst. This indicates that 1-MN was strongly adsorbed on both the Ni and Ni-Cu catalysts, whereas the adsorption of steam was promoted by the alloying of Ni with Cu. It is suggested that the Ni-Cu alloy nanoparticles might promote the dissociative adsorption of steam to form more adsorbed oxygen species, which enhanced the gasification of carbonaceous species, leading to higher activity and lower coke deposition. H_2O-TPSR of coke on the spent catalysts further demonstrated the promoting effect of Ni-Cu alloying on the steam gasification of carbonaceous species.

Acknowledgements

A part of this work was financially supported by National Nature Science Foundation of China (No. 21576052), Natural Science Foundation of Fujian Province (No. 2015J01050), Cultivation of High Level Scientific Research Achievements of Fuzhou University, as well as National High Technology Research and Development Program of China (863 Program, No. 2015AA03A402 and No. 2015AA050502).

Appendix A. Supplementary data

Supplementary data associated with this article can be found, in the online version, at http://dx.doi.org/10.1016/j.apcatb.2016.03.052.

References

[1] R.M. Navarro, M.A. Peña, J.L.G. Fierro, Chem. Rev. 107 (2007) 3952–3991.
[2] H. Lasa, E. Salaices, J. Mazumder, R. Lucky, Chem. Rev. 111 (2011) 5404–5433.
[3] Z. Abu El-Rub, E.A. Bramer, G. Brem, Ind. Eng. Chem. Res. 43 (2004) 6911–6919.
[4] M.M. Yung, W.S. Jablonski, K.A. Magrini-Bair, Energy Fuels 23 (2009) 1874–1887.
[5] D. Li, M. Tamura, Y. Nakagawa, K. Tomishige, Bioresour. Technol. 178 (2015) 53–64.
[6] J. Ashok, S. Kawi, ACS Catal. 4 (2013) 289–301.
[7] T. Furusawa, K. Saito, Y. Kori, Y. Miura, M. Sato, N. Suzuki, Fuel 103 (2013) 111–121.
[8] Y. Sekine, D. Mukai, Y. Murai, S. Tochiya, Y. Izutsu, K. Sekiguchi, N. Hosomura, H. Arai, E. Kikuchi, Y. Sugiura, Appl. Catal. A: Gen. 451 (2013) 160–167.
[9] D.A. Constantinou, A.M. Efstathiou, Appl. Catal. B: Environ. 96 (2010) 276–289.
[10] L. Di Felice, C. Courson, P.U. Foscolo, A. Kiennemann, Int. J. Hydrogen Energy 36 (2011) 5296–5310.
[11] R. Michel, A. Łamacz, A. Krzton, G. Djéga-Mariadassou, P. Burg, C. Courson, R. Gruber, Fuel 109 (2013) 653–660.
[12] A. Łamacz, A. Krztoń, G. Djéga-Mariadassou, Catal. Today 176 (2011) 347–351.
[13] J. Nishikawa, K. Nakamura, M. Asadullah, T. Miyazawa, K. Kunimori, K. Tomishige, Catal. Today 131 (2008) 146–155.
[14] L. Wang, D. Li, M. Koike, S. Koso, Y. Nakagawa, Y. Xu, K. Tomishige, Appl. Catal. A: Gen. 392 (2011) 248–255.
[15] J. Ashok, S. Kawi, Appl. Catal. A: Gen. 490 (2015) 24–35.
[16] D. Swierczynski, C. Courson, L. Bedel, A. Kiennemann, J. Guille, Chem. Mater. 18 (2006) 4025–4032.
[17] U. Oemar, P.S. Ang, K. Hidajat, S. Kawi, Int. J. Hydrogen Energy 38 (2013) 5525–5534.
[18] L. Wang, D. Li, M. Koike, H. Watanabe, Y. Xu, Y. Nakagawa, K. Tomishige, Fuel 112 (2013) 654–661.
[19] L. Wang, Y. Hisada, M. Koike, D. Li, H. Watanabe, Y. Nakagawa, K. Tomishige, Appl. Catal. B: Environ. 121–122 (2012) 95–104.
[20] M. Koike, D. Li, Y. Nakagawa, K. Tomishige, ChemSusChem 5 (2012) 2312–2314.
[21] D. Li, M. Koike, L. Wang, Y. Nakagawa, Y. Xu, K. Tomishige, ChemSusChem 7 (2014) 510–522.
[22] L. Wang, J. Chen, H. Watanabe, Y. Xu, M. Tamura, Y. Nakagawa, K. Tomishige, Appl. Catal. B: Environ. 160–161 (2014) 701–715.
[23] F. Cavani, F. Trifirò, A. Vaccari, Catal. Today 11 (1991) 173–301.
[24] K. Mette, S. Kühl, H. Düdder, K. Kähler, A. Tarasov, M. Muhler, M. Behrens, ChemCatChem 6 (2014) 100–104.
[25] D. Li, L. Wang, M. Koike, Y. Nakagawa, K. Tomishige, Appl. Catal. B: Environ. 102 (2011) 528–538.
[26] L. Wang, D. Li, H. Watanabe, M. Tamura, Y. Nakagawa, K. Tomishige, Appl. Catal. B: Environ. 150–151 (2014) 82–92.
[27] D. Li, M. Koike, J. Chen, Y. Nakagawa, K. Tomishige, Int. J. Hydrogen Energy 39 (2014) 10959–10970.
[28] D.G. Mustard, C.H. Bartholomew, J. Catal. 67 (1981) 186–206.
[29] A. Dandekar, M.A. Vannice, J. Catal. 178 (1998) 621–639.
[30] C.A. Bernardo, I. Alstrup, J.R. Rostrup-Nielsen, J. Catal. 96 (1985) 517–534.
[31] J.H. Sinfelt, J.L. Carter, D.J.C. Yates, J. Catal. 24 (1972) 283–296.
[32] T.S. Cale, J.T. Richardson, J. Catal. 79 (1983) 378–389.
[33] R. Ferrando, J. Jellinek, R.L. Johnston, Chem. Rev. 108 (2008) 845–910.
[34] I.A. Fisher, A.T. Bell, J. Catal. 178 (1998) 153–173.
[35] A. A.L, J. Inorg. Nucl. Chem. 17 (1961) 215–221.
[36] Y. Soma-Noto, W.M.H. Sachtler, J. Catal. 34 (1974) 162–165.
[37] R.K. Brandt, M.R. Hughes, L.P. Bourget, K. Truszkowska, R.G. Greenler, Surf. Sci. 286 (1993) 15–25.
[38] J. Singh, J.A. van Bokhoven, Catal. Today 155 (2010) 199–205.
[39] C.A. Leon y Leon, M. Albert Vannice, Appl. Catal. 69 (1991) 269–290.
[40] G. Delahay, D. Duprez, J. Catal. 115 (1989) 542–550.
[41] M.E.S. Hegarty, A.M. O'Connor, J.R.H. Ross, Catal. Today 42 (1998) 225–232.
[42] D. Li, Y. Nakagawa, K. Tomishige, Appl. Catal. A: Gen. 408 (2011) 1–24.
[43] D. Liu, R. Lau, A. Borgna, Y. Yang, Appl. Catal. A: Gen. 358 (2009) 110–118.
[44] D.L. Trimm, Catal. Today 49 (1999) 3–10.
[45] D.L. Trimm, Catal. Today 37 (1997) 233–238.
[46] J.H. Kim, D.J. Suh, T.J. Park, K.L. Kim, Appl. Catal. A: Gen. 197 (2000) 191–200.
[47] D. Chen, K.O. Christensen, E. Ochoa-Fernández, Z. Yu, B. Tøtdal, N. Latorre, A. Monzón, A. Holmen, J. Catal. 229 (2005) 82–96.
[48] H.S. Bengaard, J.K. Nørskov, J. Sehested, B.S. Clausen, L.P. Nielsen, A.M. Molenbroek, J.R. Rostrup-Nielsen, J. Catal. 209 (2002) 365–384.